Few-Body Systems 8, 1–10 (1990)

Few-Body Systems

Total Cross Section for the H(n, d) γ Reaction at 39, 61, and 76 MeV

P. Wauters, C. Dupont, P. Leleux, P. Lipnik, P. Macq, A. Ninane, and Sindano Wa Kitwanga

Université Catholique de Louvain, Institut de Physique Nucléaire, Chemin du Cyclotron 2, B-1348 Louvain-la-Neuve, Belgium

Abstract. The total cross section for neutron-proton capture was measured at 39, 61, and 76 MeV neutron energy with a large signal-to-background ratio. Good agreement is obtained with recent photodisintegration measurements, thus providing a critical data basis for comparison with theoretical predictions. It appears that the electric dipole approximation is still a fair description of the data.

1 Introduction

A basic process for the knowledge of the nucleon-nucleon interaction, i.e. the deuteron photodisintegration and its inverse reaction, the neutron-proton radiative capture, has gained much accuracy (both theoretically and experimentally) in the last fifteen years. The experimental total cross section, which is the subject of the present work, was indeed badly known in 1976. By that time, there was a clear disagreement between two groups measuring deuteron photodisintegration in the 15–30 MeV γ-ray energy region: Baglin et al. [1] and Weissmann and Schultz [2] on one side, yielded data that were up to 20% lower than those of Ahrens et al. [3], on the other side. Our group then started a "first-generation" measurement of the n-p capture total cross section σ_t^c between 37 and 72 MeV neutron energy; our results [4] favored the data of Ahrens et al., and also agreed with the well-admitted Partovi calculation [5]. However, this first measurement was affected by large statistical (4 to 8%) and normalization ($> 5\%$) uncertainties.

Some years later, a second measurement [7] was initiated at Louvain-la-Neuve between 45 and 70 MeV neutron energy. The σ_t^c data were then normalized to the well-known n-p elastic differential cross section at 90° center-of-mass (c.m.), which was preferred to the (less certain) cross section at extreme backward c.m. angles. The neutron-source intensity had been increased and the hydrogen target windows had been made thinner with respect to the first measurement [4]. However, in spite of these "improvements" the signal-to-background ratio was not better (0.5) than in the first measurement (0.3 to 0.5), and the statistical uncertainties remained at the 5% level. More seriously, this second set of data [7] was systematically 10% lower

than the trend of the most recent photodisintegration measurements at Frascati [8] and capture measurements at Dresden [9].

This frustrating situation led us to carry out a new measurement at three energies, in order to trace back possible systematic errors in our previous experiments [4, 7] and to clear up this problem. The present experimental set-up, which represents the end point of our ten years long committment to the field of neutron-proton capture, is described in Sect. 2. The optimization procedures and the description of the performances of the set-up are contained in Sect. 3. The data taking and analysis are treated in Sects. 4 and 5, respectively. The background subtraction problem, which is crucial for the solution of the above-mentioned discrepancy between various sets of data, is discussed in Sect. 6. Finally, the data extracted from the present work are discussed in Sect. 7.

2 The Present Experimental Set-Up

Let us first recall that, when the masses of the target and projectile are equal, the heavy product (the deuteron) is emitted in a very narrow forward cone in the laboratory (6° for $E_n = 75$ MeV); the edge of this cone corresponds to a 90° c.m. angle, while both the 0° and 180° c.m. angles are found at 0° in the lab. The deuteron angular distribution in the c.m. behaves like $a + b \sin^2 \theta_{\text{c.m.}}$, in first approximation, which means that most deuterons are emitted near the edge of the lab cone.

Deuterons are selected by a two-dimensional combination of time-of-flight (t.o.f.) and range signatures. Two detectors (plastic scintillators) are thus needed to perform the measurement: The first one (START of the t.o.f.) is thin and is located downstream with respect to the hydrogen target; the second one (STOP of the t.o.f.) is thick enough to stop the capture deuterons and is located at some distance from the START. The important point is the following: In order to detect all the capture deuterons, the scintillators should stay in the neutron beam, which unavoidably leads to a large background. The strategy applied here consisted in boring a small hole in the center of both detectors and in moving them away from the target to minimize the deuteron loss through the holes; this loss was subsequently calculated and added to the raw data. This procedure, which implied that the size of the detectors had to be increased in order to cover the whole lab deuteron cone, was not applied in our previous work: To detect the normalization protons at 45° lab, the START detector then had to be close to the target. On the other hand, the present strategy is expected to increase significantly the signal-to-background ratio.

The experimental set-up is shown in Fig. 1. The neutrons were produced by the ^{7}Li(p, n) reaction [6]. The width of the cyclotron beam bursts was reduced to about 1 ns FWHM using a narrow slit near the cyclotron center. A 10 μA proton beam of 42, 65 or 80 MeV bombarded a 0.5 or 1 cm thick natural lithium target. Protons were bent afterwards by a few cm, and stopped in a graphite Faraday cup; the target and beam stop were heavily shielded. The neutrons at 0° were guided through a conical iron or brass collimator made of three separate parts: The first one was 1.6 m long, started immediately behind the Faraday cup and had an initial diameter of 10 mm; the second one was 60 cm long, started 4.7 m from the Li target, and had a final diameter of 17.1 mm (this part was made of brass, inserted in the gap of a dipole magnet); the third one was 80 cm long and served as an anti-halo collimator,

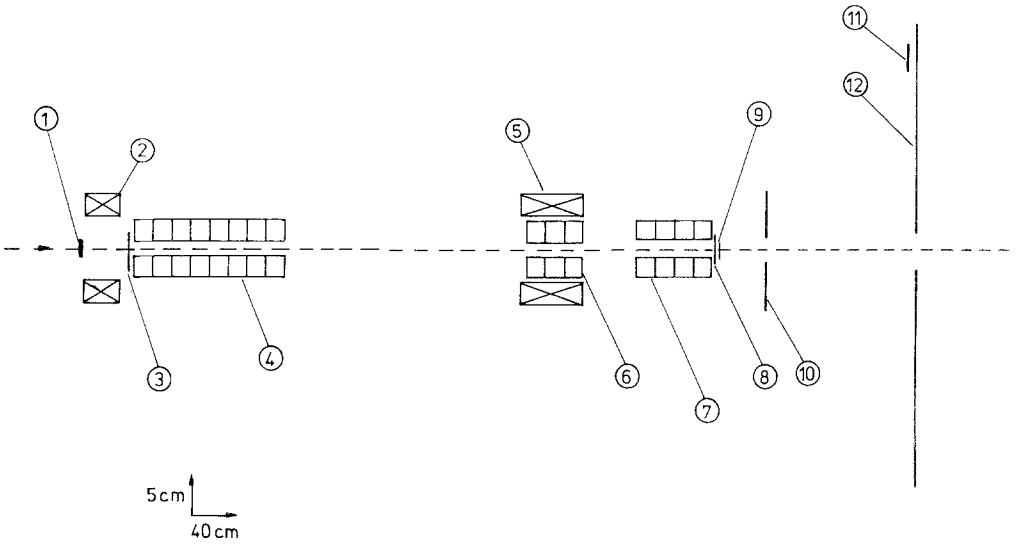

Fig. 1. Experimental set-up used in the present work. Encircled numbers refer to the following items: ① Li target, ② proton bending magnet, ③ proton beam stopper, ④ first part of the neutron collimator, ⑤ dipole magnet, ⑥ second part of the collimator, ⑦ anti-halo collimator, ⑧ ANTI detector, ⑨ liquid hydrogen target, ⑩ START detector, ⑪ PROTON detector, ⑫ STOP detector

i.e. it was designed to absorb neutrons scattered inside the end of the second part of the collimator [9].

The collimator defined a 20 mm diameter neutron beam at 6.7 m from the Li target. At that place, neutrons interacted with a liquid hydrogen target, limited by two 35 mm diameter and 6 μm thick aluminized mylar windows. Charged particles coming out of the target were detected and identified by two plastic scintillators. The first one (START) was a thin (0.2 mm) NE102 foil, 16 cm diameter, located at 50 cm from the hydrogen target; a 3 cm diameter hole was bored in its center and it was viewed by two fast (XP2020) photomultipliers (PM). The second scintillator (STOP) was a thick (1.5 cm) NE102 plate, of 68 × 64 cm^2 surface, located at 1.57 m from the START detector; a 5 cm hole was bored in its center, and 8 PM (4 on each of two opposite sides) were linked to this scintillator in order to maximize the light collection. In front of the STOP detector (but outside the expected impact surface of the capture deuterons), a small plastic detector (PROTON), 12 × 3 cm^2 size and 4 mm thick, detected protons scattered at a 7° lab angle. The whole set-up, including the neutron path, was kept under vacuum. A capacitive beam pick-off (BPO), located upstream with respect to the Li target, detected the passage of the cyclotron beam bursts. In front of the hydrogen target, a thin (0.1 mm) plastic scintillator (ANTI) vetoed by anticoincidence the charged particles possibly contaminating the neutron beam.

3 Study and Optimization of the Set-Up

3.1 The START and STOP Detectors

The thin (0.2 mm) START detector was linked to two PM. The average time of arrival of the two PM pulses was taken to derive a timing signal from this detector.

The STOP scintillator was viewed by eight PM. The amplitude response was optimized by moving a gamma-ray source over the whole scintillator surface and requesting that the total number of counts of the eight PM be independent of the source position (the relative variation was less than 0.4%). The time response was measured for different combinations of the timing signals derived from the eight PM, using protons from *n-p* scattering; the best resolution of the START-STOP t.o.f. (1.5 ns) was obtained by taking the arithmetic mean of the eight PM timing signals.

The loss of deuterons through the holes in the detectors were calculated by a Monte-Carlo simulation of the emission of deuterons from the target into the set-up, with an angular distribution taken from a global fit of the previous data [10]; this deuteron loss was 2.3% at 39 MeV and 1.7% at 61 and 76 MeV. These percentages are small and are compensated by the large decrease of the deuteron background, caused by the holes in the detectors.

3.2 The Charged Particles in the Neutron Beam

The ANTI detector was designed to suppress the charged particles in the neutron beam. Unfortunately, the neutrons passing through this detector produced charged particles which, if originating from the back layers of the detector, were not vetoed: The deuteron background (i.e. the number of deuterons recorded with an empty hydrogen target) was indeed smaller by 60% without this detector. Consequently, it was taken out of the set-up. A subsequent measurement of the charged particles contamination in the neutron beam was carried out at 39 MeV by inserting a dipole magnet between the hydrogen container (a copper frame with a 35 mm hole and no windows) and the START detector; this magnet deflected the charged particles into the START and STOP detectors. These charged particles (deuterons and protons) amounted to less than 10^{-5} and 10^{-8} of the *n-p* capture deuterons and of the *n-p* elastic protons, respectively. As a further check, a capture measurement was carried out with and without the ANTI detector: The ratios N_d/N_p of the capture deuterons to the elastic protons were (0.302 ± 0.002) (with) and (0.305 ± 0.004) (without) at 61 MeV, and (0.285 ± 0.004) and (0.291 ± 0.003) at 76 MeV; this shows that the final results were not significantly affected by charged particles in the neutron beam.

3.3 The Effect of the Anti-Halo Collimator

When the third part of the collimator, i.e. the anti-halo collimator, was replaced by a classical collimator, i.e. four 20 cm long iron pieces with a central hole increasing from 17 mm up to 20 mm, the background was then increased by a factor of three. This illustrates the need for a correct handling of the neutron beam near the target.

4 Data Taking

Standard fast electronics was used to construct, from the PM anode signals, two different types of logical gates, the first one corresponding to particles passing through the START and STOP detectors, and the second one, to particles passing through the START, STOP, and PROTON detectors. A very narrow START signal

was finally put in coincidence with the two types of gates, in order: (i) to define precisely the gate timing (which was also the start of the t.o.f. measurements); and (ii) to reject elastic protons (which were much more numerous than the deuterons) in the first type of gates by adjusting the relative delays in this coincidence. An OR signal constructed with these two gates was used to activate CAMAC modules, i.e. ADC's receiving the amplitude signals and TDC's processing the timing signals from all the PM and from the BPO. CAMAC events were transferred to a magnetic tape via a PDP 11-34 computer.

Alternate measurements were carried out with a filled or an empty hydrogen target, and they were normalized to the integrated proton beam current.

5 Data Analysis

The STOP amplitude and the START-STOP t.o.f. were combined in a two-dimensional spectrum of energy versus time, in which particles of different masses were clearly separated (Fig. 2), so that deuterons could be selected. The START-PROTON t.o.f. spectrum was also constructed, which contained mostly protons from n-p scattering. Deuterons in the former spectrum and protons in the latter resulted from interactions of all the neutrons produced in the p + Li reaction. If one wishes to derive a capture total cross section at a definite neutron energy, one has to select a neutron energy bin, i.e. the high-energy peak in the neutron spectrum resulting from the ^{7}Li(p, n)^{7}Be(0 + 0.47 MeV) reaction. The *measured* neutron spectrum (BPO-START t.o.f. (t'_n)) was of course deformed by the difference in the times-of-flight between the hydrogen target and the START detector. The *exact* neutron t.o.f. (t_n) was thus calculated as the difference between the measured t.o.f. (t'_n) and the START-STOP or START-PROTON t.o.f. (t''_n), corrected for the ratio of the hydrogen target to the START detector distance (d_1), and the START-STOP or START-PROTON distance (d_2):

$$t_n = t'_n - t''_n \frac{d_1}{d_2}.$$

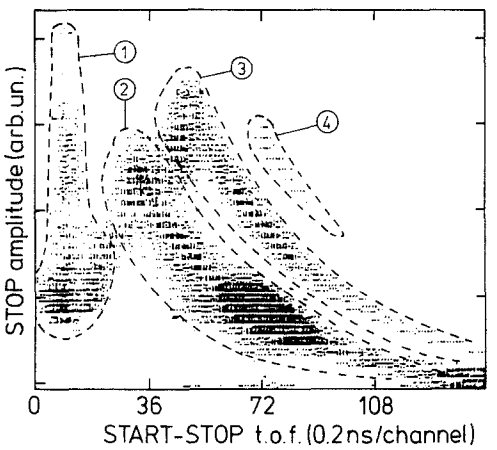

Fig. 2. Two-dimensional spectrum (the STOP amplitude versus the START-STOP t.o.f.) at 76 MeV neutron energy for a filled hydrogen target. Different parts of the spectrum are separated by dotted curves and indicated by numbers: ① = protons passing through the STOP detector, ② = protons stopped in the STOP detector, ③ = deuterons, ④ = tritons. The t.o.f. scale is 0.2 ns/channel. The STOP amplitude is in arbitrary units. The large stain in zone ② is due to n-p elastic scattering induced by low-energy neutrons having a t.o.f. equal to the t.o.f. of the high-energy neutron peak plus one RF period between the BPO and the START. Capture deuterons appear around channel 72 in zone ③

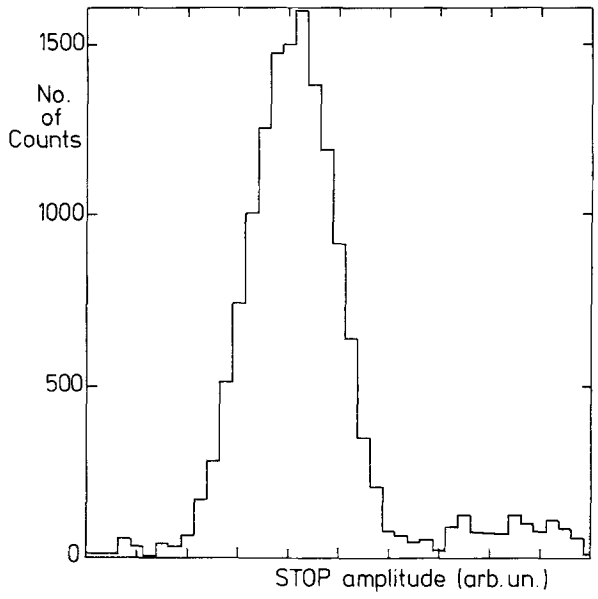

Fig. 3. Deuteron energy spectrum at 61 MeV neutron energy, resulting from the projection on the vertical axis of zone ③ of two-dimensional spectra like the one in Fig. 2) (after high-energy neutrons had been selected). Fig. 3 is a difference spectrum (filled minus empty target)

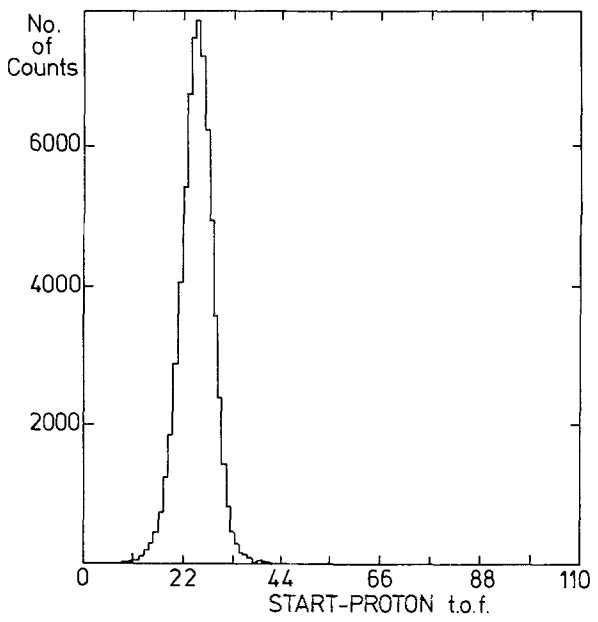

Fig. 4. START-PROTON t.o.f. spectrum obtained after selection of the high-energy neutrons. The abscissa scale is 0.2 ns/channel

Once this exact neutron t.o.f. was reconstructed for the deuterons and for the normalization protons, it was important to select, in both spectra, the *same* energy region. Having done that, the above-mentioned two-dimensional spectrum and the START-PROTON t.o.f. spectrum were again reconstructed. The deuteron region in the former (Fig. 3) and the proton high-energy peak (corresponding to *n-p* scattering induced by the high-energy neutron peak) in the latter (Fig. 4) were integrated, thereby yielding the N_d/N_p ratio.

6 The Background Subtraction

Only the deuteron spectra were considered in the background subtraction procedure; for the normalization protons (elastic scattering), the background was indeed negligible. The deuteron background spectrum was measured during the runs with an empty target, while the "signal-plus-background" spectrum was obtained from the runs with a filled hydrogen target. Unfortunately, the filled and empty target energy spectra cannot be subtracted directly, owing to the energy shift caused by the liquid hydrogen on the background produced upstream of the liquid hydrogen (e.g., in the entrance window of the target). This energy shift was clearly visible in the deuteron energy spectra for the filled and empty target (Fig. 5). The energy distribution and the amount of the background to be shifted were unknown. The energy distribution was thus assumed to be uniform, and the amount was adjusted by requesting that the STOP and START energy difference spectra be as close to

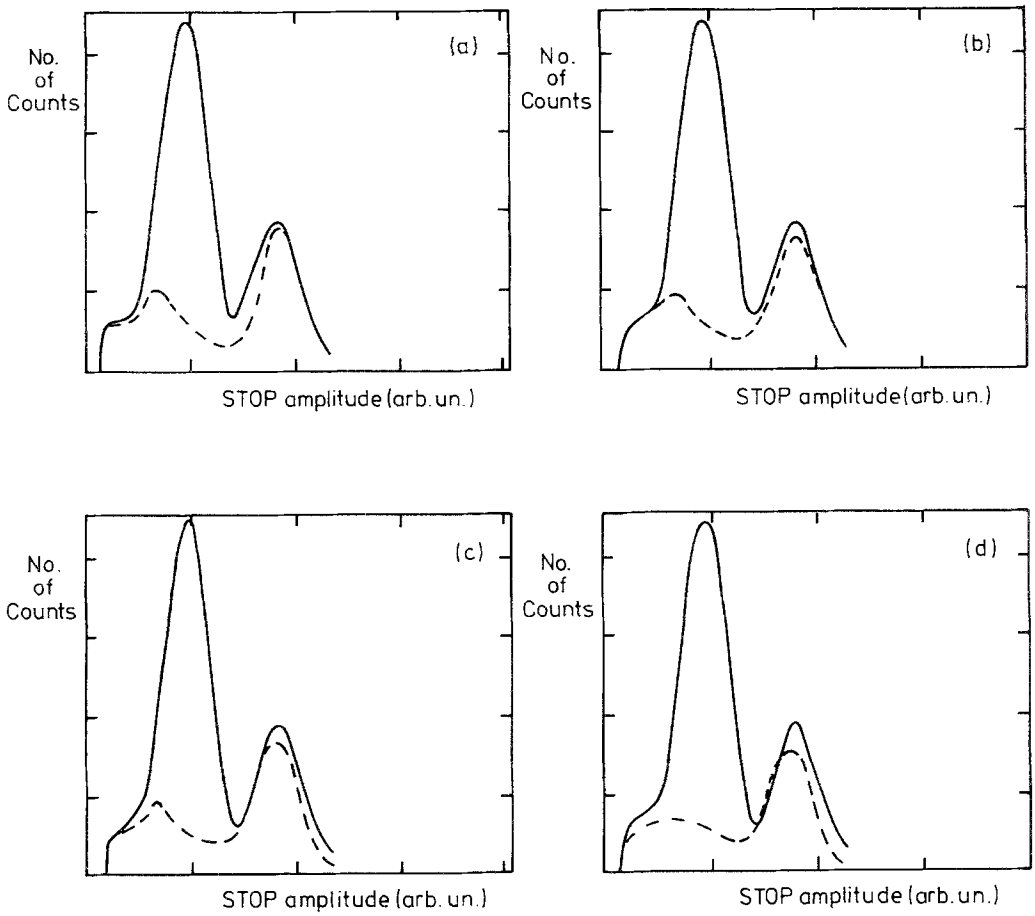

Fig. 5. **a**: Deuteron energy spectra at $E_n = 61$ MeV for the filled target (signal plus background; solid curve) and the empty target (background; dashed curve). The capture deuteron peak is dominant in the filled target spectrum, and the energy shift is clearly visible in the high-energy background. **b**, **c**, **d**: A fixed percentage of the background, uniformly scattered over all the energy spectrum, has been shifted: 30% (**b**), 50% (**c**), 70% (**d**). The best subtraction of the two spectra on both sides of the capture-deuteron peak is obtained in **c**

zero as possible on both sides of the capture-deuteron region after the shift. The signal-to-background ratio being rather large in the present work (3.0 at 39 MeV, 3.1 at 65 MeV, and 1.6 at 76 MeV), the capture-deuteron number (N_d) changed by 5% at most when varying the percentage of the shifted background from 0 to 70% of the total background.

However, a reexamination of our previous data [7] (where the signal-to-background ratio was ~ 0.5) showed that in that experiment a shift of only 10% in the amount of background increased the deuteron number (and thus the capture cross section) by 8%. Due to the fact that in our previous work the START and STOP detectors were staying in the neutron beam, we had conjectured that most of the background was created downstream of the hydrogen target, and the background subtraction problem had not been taken into account. It now appears that our previous data were affected by a systematic error, which was corrected for in the present work.

7 Results and Discussion

The deuteron number N_d, obtained from the integration of the capture deuteron peak in the STOP amplitude spectrum, had to be corrected for two effects, i.e. the deuteron-induced nuclear reactions in the STOP scintillator (the t.o.f. is correctly measured but the amplitude is not), and the deuteron loss through the holes of the START and STOP detectors. The first correction was measured [11], and was shown to be smaller than $3.3 \pm 0.2\%$; the second one was calculated by a Monte-Carlo program (see Sect. 3), and was found to be smaller than $2.3 \pm 0.2\%$. The statistical error (one standard deviation) on the N_d/N_p ratio is 1.9% at 38 MeV and 1.2% at 61 and 76 MeV.

The capture total cross section σ_t^c is related to the deuteron-to-proton ratio N_d/N_p by the formula

$$\sigma_t^c = \frac{N_d}{N_p} \cdot \frac{d\sigma}{d\Omega}(7^\circ)\, \Delta\Omega,$$

where $d\sigma/d\Omega\ (7^\circ)$ is the n-p elastic scattering cross section for protons scattered at 7° in the lab, and $\Delta\Omega$ is the lab solid angle of the proton detector.

The n-p elastic cross sections at 39, 61, and 76 MeV were extracted from a recent global phase-shift analysis [12] (Table 1). The uncertainty in this cross section is smaller than 5%.

Fig. 6 shows the n-p capture cross sections measured in this work, translated into photodisintegration cross sections and, to get rid of its steep variation with energy, normalized to the electric-dipole cross section σ_{E1},

$$\sigma_{E1} = \frac{8\pi}{3} \frac{1}{\gamma^2} \left(\frac{\gamma k}{\gamma^2 + k^2} \right)^3 \frac{1}{1 - \gamma r_{ot}},$$

where γ is the inverse of the spatial extension of the deuteron (0.232 fm^{-1}), $r_{ot} =$ 1.75 fm is the triplet-state effective range, and k is the nucleon wave number. Our data are compared in Fig. 6 with recent capture [9], or photodisintegration [3], [8] measurements. Only statistical uncertainties were drawn. The data of refs. [1] and [2] were not plotted, as they would be out of the scale (downwards) for some of

Table 1. Measurements of the n-p capture total cross section (σ_t^c) from this work, translated into the photodisintegration cross section σ_t^{ph}, at the equivalent gamma-ray energy E_γ. The third column yields the n-p elastic scattering cross section $d\sigma/d\Omega$ (7°) used to normalize our data

$E_n \pm \Delta E_n$ [a] (MeV)	$E_\gamma \pm \Delta E_\gamma$ (MeV)	$d\sigma/d\Omega$ (7°) (mb/sr)	σ_t^c [b] (μb)	σ_t^{ph} (μb)
38.5 ± 1.9	21.5 ± 1.0	22.04	20.62 ± 0.39	550.3 ± 10.5
60.8 ± 2.5	32.6 ± 1.3	15.46	16.62 ± 0.20	370.0 ± 3.7
76.2 ± 2.1	40.3 ± 1.1	13.50	14.13 ± 0.19	215.8 ± 2.6

[a] Energy width calculated from the energy loss of the proton beam in the lithium target

[b] Only the statistical errors are quoted

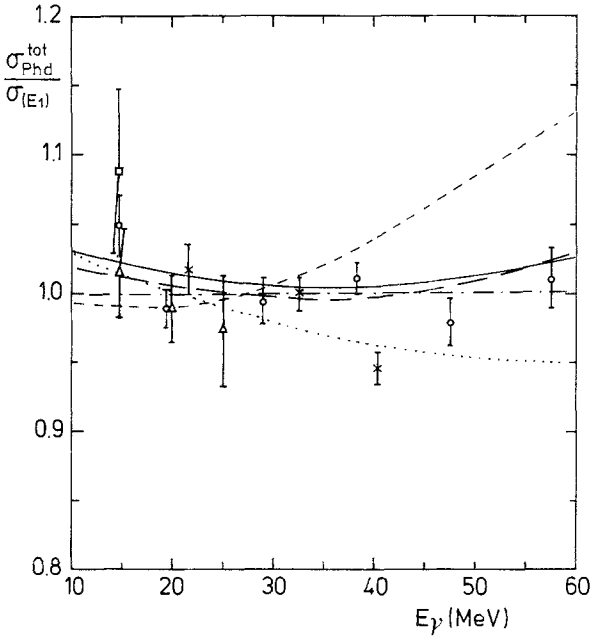

Fig. 6. Data obtained in this work (crosses), normalized to the electric-dipole cross section, and expressed in terms of photodisintegration via the detailed-balance theorem, versus the equivalent gamma-ray energy ($E_\gamma = E_n/2 + 2.2$ MeV). The triangles and the open dots are the data of refs. [3] and [8], respectively, the open square is the result of ref. [9]. The curves are the results of the calculations of ref. [13] (dashed line), ref. [14] (solid line), ref. [15] (dashed-dotted line), ref. [16] (long-dashed line), and ref. [17] (dotted line)

them. The normalization uncertainty on our data is at most 5%. The quoted systematic errors are 2 to 3% on the data of ref. [8] and 2 to 4% on the data of ref. [3]. At 22 and 32 MeV, the agreement between our data and the previous measurements is excellent. Such is not the case for the 40 MeV data point. We have to admit, however, that at this energy our set-up was reaching its ultimal performance. The STOP detector was indeed not thick enough to stop all the background deuterons and protons from the $n + {}^{12}C$ reactions; the deuteron and proton hyperbolae in the two-dimensional spectrum had thus on their left end a ΔE branch which prevented us from obtaining a very clear separation between protons and deuterons in the high-energy part of the spectrum; the signal-over-background ratio was only 1.5 at this energy instead of 3.0 at the two lower energies. We estimate that the additional uncertainity at 40 MeV is at the 5% level and we strongly believe that from this third

data point one should not conclude that the cross section shows a definite trend downwards at high energy.

Also plotted in Fig. 6 are the results of theoretical calculations of Rustgi et al. [13], Jaus and Woolcock [14], Lucio et al. [15], Arenhövel [16] and Laget [17]. The original work of Partovi [5], which was not drawn for clarity, would remain very close to the $E1$ effective-range approximation over the 10–60 MeV energy range (the relative difference being smaller than 2%). As the main goal of the present work was to solve an experimental discrepancy, we refer to the recent paper of Jaus and Woolcock [14] for a thorough discussion of the theoretical situation. It appears from Fig. 6 that the electric-dipole cross section remains a good approximation for the set of the most recent data, and that precise measurements above 40 MeV γ-ray energy (or 80 MeV neutron energy) would be helpful to discriminate between the various calculations. It should be pointed out, however, that the capture reaction will be less attractive at those energies because: (i) the n-p normalization cross section is less precisely known; and (ii) the detailed balance factor, which connects the capture and photodisintegration cross sections, will be more and more in favour of the latter.

Acknowledgement. We wish to thank the cyclotron crew, the electronics and mechanics workshops, and the computer group of the Nuclear Physics Department. This work was sponsored by the Interuniversity Institute for Nuclear Sciences, Belgium. One of us (P. Leleux) is a Research Associate of the National Fund for Scientific Research, Belgium.

References

1. Baglin, J. E. E., Carr, R. W., Bentz Jr., E. J., Wu, C.-P.: Nucl. Phys. **A201**, 593 (1973)
2. Weissmann, B., Schultz, H. L.: Nucl. Phys. **A174**, 129 (1971)
3. Ahrens, J., Eppler, H. B., Gimm, H., Kröning, M., Riehn, P., Wäffler, H., Zieger, A., Ziegler, B.: Phys. Lett. **52B**, 49 (1974)
4. Bosman, M., Leleux, P., Lipnik, P., Macq, P., Ninane, A.: Phys. Lett. **82B**, 212 (1979)
5. Partovi, F.: Ann. of Phys. **27**, 79 (1964)
6. Bol, A., Leleux, P., Lipnik, P., Macq, P., Ninane, A.: Nucl. Instr. Meth. **214**, 169 (1983)
7. Dupont, C., Leleux, P., Lipnik, P., Macq, P., Ninane, A.: Nucl. Phys. **A445**, 13 (1985)
8. Bernabei, R., Incicchitti, A., Mattioli, M., Picozza, P., Prosperi, D., Casano, L., d'Angelo, S., De Pascale, M. P., Schaerf, C., Giordano, G., Matone, G., Frullani, S., Girolami, B.: Phys. Rev. Lett. **57** 1542 (1986)
9. Stiehler, T., Kühn, B., Möller, K., Mössner, J., Neubert, W., Pilz, W., Schmidt, G.: Phys. Lett. **151B**, 185 (1985)
10. De Pascale, M. P., Giordano, G., Matone, G., Picozza, P., Azario, L., Caloi, R., Casano, L., Ingrosso, L., Mattioli, M., Poldi, E., Prosperi, D., Schaerf, C.: Phys. Lett. **119B**, 30 (1982)
11. Gilot, J.-F., Bol, A., Leleux, P., Lipnik, P., Macq, P.: Nucl. Instr. Meth. **188**, 305 (1981)
12. Arndt, R. A.: SAID Program (Solution SM87) (private communication)
13. Rustgi, M. L., Reeta, V., Rustgi, O. P.: Phys. Rev. **C29**, 785 (1984)
14. Jaus, W., Woolcock, W. S.: Nucl. Phys. **A473**, 667 (1987)
15. Lucio, J. L., Martinez, A., Pestieau, J.: Nuov. Cim. **89A**, 292 (1985)
16. Arenhövel, H.: Private communication (1988)
17. Laget, J. M.: Private communication (1988)

Received August 31, 1989; revised November 3, 1989; accepted for publication November 13, 1989